Semiclassical canonical rate theory

Eli Pollak* and Bruno Eckhardt
Fachbereich Physik der Philipps, Universität Marburg, Renthof Strasse 6, D-35037 Marburg, Germany
(Received 22 May 1998)

The exact quantum rate may be represented as a phase space trace of a product of two operators: the symmetrized thermal flux operator and a projection operator onto the product space. A semiclassical analysis of the phase space representation of these two operators is presented and used to explain recent results found for a quantum thermodynamic rate theory. For low temperatures, the central object that is responsible for the oscillatory nature of the flux operator is a periodic orbit on the upside down potential surface whose period is $2\hbar/k_BT$. The semiclassical analysis of the flux distribution explains why a variation of the dividing surface leads to improved thermodynamic rate estimates in asymmetric systems. The semiclassical limit (stationary phase limit) of the projection operator is shown to be identical to the classical projection operator. A semiclassical rate theory is obtained using the product of the semiclassical flux distribution and either the parabolic barrier or the classical projection operator and compared with the exact rate and approximate quantum thermodynamic estimates. [S1063-651X(98)13310-X]

PACS number(s): 03.65.Sq, 31.70.Hg, 82.20.Pm

I. INTRODUCTION

The quantum theory of reaction rates [1] is almost as old as quantum mechanics itself, but even at the turn of this century it presents some formidable challenges. During the past two decades one could broadly identify two approaches. One is to recognize the difficulty in obtaining exact quantum rate expressions except for some special cases, such as a parabolic barrier, and proceed to find the numerically exact quantum rate. This approach has seen dramatic advances during the past decade and one now can almost routinely obtain numerically exact rates for systems with three degrees of freedom [2].

A second approach, especially important for the condensed matter community, was to replace rigor with reasonable approximations. A strategy that has gained much popularity in recent years is to estimate quantum rates using centroid densities [3,4]. Since a centroid density is a thermodynamic object, it can be readily estimated using Monte Carlo path integral techniques [5].

Another major class of approximation methods may be thought of as mixed classical quantum propagation techniques. Since time-dependent numerical methods for systems with two or three degrees of freedom are available, it makes sense to treat the quantum dynamics of a few degrees of freedom exactly and treat the rest classically. The semiclassical theory of reaction rates has also been resurrected in recent years. Various researchers [6,7] have noted that much of the quantum dynamics may be accounted for by suitable integration of semiclassical approximations to the real time propagator. This approach has recently raised the question as to whether quantum tunneling could be accounted for semiclassically by considering only real time trajectories. Keshavamurthy and Miller [8] showed that real time trajectories account for much of the tunneling, but Maitra and Heller [9,10] argued that deep tunneling can only be described with the added help of imaginary time trajectories across the barrier.

One way of getting a semiclassical theory of thermal rates is by considering the semiclassical microcanonical theory and then averaging over the canonical distribution. This approach was used by Hänggi and Hontscha [11] to derive an expression for the thermal rate valid at all temperatures. They based themselves on Miller's semiclassical transition state theory [12], which in turn is based on Wigner's approximate rate expression [13].

In this paper we choose a different starting point: the exact thermal rate expression as derived by Miller, Schwartz, and Tromp [14] and used [15] by Thompson and Miller,

$$k(T)=Q_r(T)^{-1}\lim_{t\to\infty} C_{\rm FS}(t), \tag{1.1}$$

where $C_{\rm FS}(t)$ is the so-called flux side correlation function, which may be written in the form

$$C_{\rm FS}(t)={\rm tr}[\hat{F}(\beta,q_{DS})P(t)]. \tag{1.2}$$

The quantum projection operator $P(t)$ is defined as

$$P(t)=e^{i\hat{H}t/\hbar}\hat{h}(\hat{q})e^{-i\hat{H}t/\hbar} \tag{1.3}$$

and $\hat{h}$ is the step function operator, which (in the space representation) is unity on the product side ($q>0$) and is zero on the reactant side ($q<0$). $\hat{F}(\beta,q_{DS})$ is the symmetrized quantum thermal flux operator at the dividing surface defined by q_{DS},

$$\hat{F}(\beta,q_{DS})=e^{-\beta\hat{H}/2}\hat{F}(q_{DS})e^{-\beta\hat{H}/2}, \tag{1.4}$$

and $\hat{H}$ is the Hamiltonian operator of the system. The symmetrized flux operator $\hat{F}(q_{DS})$ (in one dimension) is

$$\hat{F}(q_{DS})=\frac{1}{2m}[\hat{p}\,\delta(\hat{q}-q_{DS})+\delta(\hat{q}-q_{DS})\hat{p}], \tag{1.5}$$

*Permanent address: Chemical Physics Department, Weizmann Institute of Science, 76100 Rehovot, Israel.

$Q_r(T)$ is the reactants partition function at temperature T, and $\beta = 1/k_B T$.

In Miller's rate expression all the dynamics is hidden in the infinite time limit of the projection operator

$$P \equiv \lim_{t\to\infty} P(t) = \lim_{t\to\infty} e^{i\hat{H}t/\hbar}\hat{h}(\hat{q})e^{-i\hat{H}t/\hbar}. \tag{1.6}$$

Obtaining the exact rate necessitates a real time propagation. A numerically exact solution is feasible for systems with a few degrees of freedom [15–20], but there is still a way to go before one can rigorously implement the time evolution in a liquid.

In a recent publication [21] it was noted that Miller's exact rate expression could be recast as a phase space trace of the Wigner representation [22] of the product of the projection operator and the symmetrized thermal flux operator. The Wigner representation of an operator is defined as

$$O(p,q) = \frac{1}{2\pi\hbar}\int_{-\infty}^{\infty} d\xi\; e^{ip\xi/\hbar}\langle q - \tfrac{1}{2}\xi|\hat{O}|q + \tfrac{1}{2}\xi\rangle. \tag{1.7}$$

The exact expression for the quantum rate may thus be written formally as

$$k(T) = Q_r(T)^{-1} 2\pi\hbar \int_{-\infty}^{\infty} dp\; dq\; P(p,q)F(p,q;\beta,q_{DS}). \tag{1.8}$$

A quantum transition state theory (QTST) was then formulated, in which one replaces the exact projection operator with its leading-order approximation obtained by considering only the dynamics of the parabolic barrier. Alternatively, it was suggested [21] that one could replace the quantum projection operator with its classical limit, thus giving a mixed quantum classical theory (MQCLT), in which the flux operator is evaluated exactly and the projection operator is obtained from classical trajectories.

Both theories were studied in some detail in Refs. [21] and [23]. It was shown in Ref. [21] that the accuracy of QTST is comparable to that of the centroid method. QTST invariably gives a numerical upper bound for the quantum rate, whose accuracy deteriorates with decreasing temperature and increasing asymmetry of the potential. The MQCLT approach gives an improvement, but not a very big one. The MQCLT approach was also subsequently implemented in Ref. [24].

An interesting feature of both theories is their variational property [21]. A variation of the location of the dividing surface, looking for the point at which the approximation is stationary, leads to significant improvement in the case of asymmetric systems [23].

These studies pose a few challenges. Why does QTST give an upper bound? Why is the variation of the dividing surface useful and is it at all clear that one will really find an extremum of the reactive flux with respect to the dividing surface? What is needed to improve the QTST and MQCLT theories so that they will become quantitative even in the deep tunneling region? The perturbation theory analysis presented in Ref. [23] indicated that a smearing of the classical Heaviside function is important, but how does this come about? Can one obtain a good quantum approximation for the projection operator?

In this paper we will provide a semiclassical analysis of the phase space structure of the symmetrized flux operator and the projection operator. In Ref. [23] we found that for deep tunneling, the thermal flux distribution becomes rather delocalized in momentum, with positive and negative peaks. The variational flux distribution had the same qualitative structure, irrespective of the symmetry of the potential. A semiclassical theory for the flux distribution that explains these features is presented in Sec. II. The variational aspect is also explained; the optimal location of the dividing surface is the one for which the two trajectories that contribute to the symmetrized thermal flux operator join smoothly. The central object of the flux distribution is thus a periodic orbit on the inverted potential, whose period is $2\hbar\beta$ (the factor of two is not a misprint) and only *half* of its full action contributes to the flux.

The semiclassical theory of the projection operator is studied in Sec. III. The idea that one could derive the semiclassical limit of the projection operator would, at first sight, seem strange. The projection operator has in it an infinite time limit and any semiclassical time-dependent approach is expected to fail for infinitely long times. Note, however, that for a parabolic barrier, the semiclassical limit of the projection operator is exact, even though here too one resorts to an infinite time limit. This is a reflection of the fact that the semiclassical propagator takes into account the quadratic fluctuations around the classical path and for a parabolic potential this is all that matters. The generic potential $V(q)$ has a parabolic form at the barrier, while as $q\to\infty$ or as $q\to -\infty$ the potential goes to a constant, where again the semiclassical propagator is exact. The semiclassical propagator is thus exact except for the nonharmonic region of the potential where the particle spends typically a short time. For short time dynamics the semiclassical approximation is actually good and one might expect a semiclassical theory to be quite useful. We find that the semiclassical limit of the Wigner distribution function of the projection operator is just the classical projection operator.

A remarkable semiclassical picture thus emerges from this theory. The amplitude of the flux distribution in the deep tunneling region is reduced by only half of the action of the imaginary time periodic orbit whose period is $2\hbar\beta$. This action is substantially less than the full instanton action of the periodic orbit with period $\hbar\beta$ that appears in the standard semiclassical treatments of thermal reaction rates [1]. Indeed, an upper bound for the rate, based on only the flux distribution, gives an estimate that is approximately the square root of the exact transmission coefficient [25]. The flux distribution is not positive definite and it is the combination of the two operators that gives the tunneling rate. The relatively large positive peaks of the flux distribution are almost entirely canceled by the negative peaks. The projection operator defines the regions of phase space that contribute most. As the temperature is lowered, the flux distribution delocalizes and it is the combination of this delocalization and the projection operator that leads to the net rate. The semiclassical rate theory that emerges from the combination of the two operators is presented in Sec. IV and applied to the symmet-

ric Eckart barrier. We end in Sec. V with a further discussion of the implications of the present theory on our understanding of quantum tunneling.

II. THE SEMICLASSICAL SYMMETRIZED THERMAL FLUX OPERATOR IN PHASE SPACE

A. Preliminaries

For a particle with mass m the one-dimensional Hamiltonian operator $\hat{H}$ is

$$\hat{H}=\frac{1}{2m}\,\hat{p}^2+V(\hat{q}). \tag{2.1}$$

Without loss of generality, the potential V may be divided into a parabolic barrier and a nonlinear term

$$V(q)=V^{\ddagger}-\tfrac{1}{2}m\omega^{\ddagger 2}q^2+V_1(q) \tag{2.2}$$

such that the barrier is located at $q=0$. The matrix elements of the symmetrized thermal flux operator may be expressed [14,21] in terms of matrix elements of the thermal density operator $e^{-\beta\hat{H}}$:

$$\begin{aligned}\langle q''|\hat{F}(\beta,q_{DS})|q'\rangle &= \frac{i\hbar}{2m}\left(\left\langle q''|e^{-\beta\hat{H}/2}|\,\frac{\partial}{\partial q_{DS}}\right\rangle\langle q_{DS}|e^{-\beta\hat{H}/2}|q'\rangle\right.\\ &\quad\left.-\langle q''|e^{-\beta\hat{H}/2}|q_{DS}\rangle\left\langle\frac{\partial}{\partial q_{DS}}\,|e^{-\beta\hat{H}/2}|q'\right\rangle\right),\end{aligned} \tag{2.3}$$

where we used the shorthand notation

$$\left\langle q''\left|e^{-\beta\hat{H}/2}\right|\,\frac{\partial}{\partial q_{DS}}\right\rangle\equiv\left(\frac{\partial}{\partial q}\,\langle q''|e^{-\beta\hat{H}/2}|q\rangle\right)_{q=q_{DS}}. \tag{2.4}$$

The Wigner representation of the symmetrised thermal flux operator is then by definition

$$\begin{aligned}F(p,q;\beta,q_{DS}) &= \frac{i}{4m\pi}\int_{-\infty}^{\infty}d\xi\; e^{i(p\xi/\hbar)}\left(\left\langle q-\frac{\xi}{2}\right|e^{-(\beta/2)\hat{H}}\left|\frac{\partial}{\partial q_{DS}}\right\rangle\right.\\ &\quad\times\left\langle q_{DS}\left|e^{-(\beta/2)\hat{H}}\right|q+\frac{\xi}{2}\right\rangle-\left\langle q-\frac{\xi}{2}\,\right|e^{-\beta\hat{H}/2}\left|q_{DS}\right\rangle\\ &\quad\left.\times\left\langle\frac{\partial}{\partial q_{DS}}\right|e^{-(\beta/2)\hat{H}}\left|q+\frac{\xi}{2}\right\rangle\right).\end{aligned} \tag{2.5}$$

The semiclassical approximation for a matrix element of the thermal density matrix is [26]

$$\begin{aligned}\langle q''|e^{-(\beta/2)H}|q'\rangle_{\rm sc}&=\left(2\pi\hbar\left|\frac{\partial q''}{\partial p'}\right|\right)^{-1/2}e^{-S(q'',q')/\hbar}\\ &\equiv A(q'',q')e^{-S(q'',q')/\hbar},\end{aligned} \tag{2.6}$$

where the action $S(q'',q')$ is that of a classical trajectory moving on the upside down potential with energy E, which was initiated at time $t=0$ at the point q' and ended up at time $\hbar\beta/2$ at the point q'':

$$S(q'',q')=\int_{q'}^{q''}dq\;p(q)-\tfrac{1}{2}\hbar\beta E. \tag{2.7}$$

The momentum p' in the prefactor of Eq. (2.6) is the initial momentum of the trajectory. If more than one classical trajectory obeys the double ended boundary conditions then one must sum over the contribution of all such trajectories.

The rate expression has in it derivatives of the thermal density matrix element. We note that

$$\frac{\partial S(q'',q')}{\partial q'}=-p', \tag{2.8}$$

$$\frac{\partial S(q'',q')}{\partial q''}=p''. \tag{2.9}$$

The derivative of the prefactor may be ignored since in the context of the semiclassical approximation it will only lead to small correction terms. Therefore, we may write down the Wigner representation of the thermal flux operator as

$$\begin{aligned}F(p,q;\beta,q_{DS}) &\simeq \frac{i}{4m\pi\hbar}\int_{-\infty}^{\infty}d\xi\;e^{i(p\xi/\hbar)}\left[p_i\left(q-\frac{\xi}{2},q_{DS}\right)\right.\\ &\quad\left.-p_i\left(q+\frac{\xi}{2},q_{DS}\right)\right]A\left(q-\frac{\xi}{2},q_{DS}\right)\\ &\quad\times A\left(q+\frac{\xi}{2},q_{DS}\right)e^{-(1/\hbar)[S(q+\xi/2,q_{DS})+S(q-\xi/2,q_{DS})]},\end{aligned} \tag{2.10}$$

where we used the fact that the action and the prefactor are symmetric with respect to time reversal of the trajectory [$S(x,x')=S(x',x)$ and $A(x',x)=A(x,x')$]. The momentum $p_i(q',q)$ is the initial momentum of the trajectory that was initiated at time $t=0$ at the point q and reached the point q' at the time $\hbar\beta/2$.

B. The optimal tunneling path

To understand the structure of the flux distribution in phase space, one should look for those regions in phase space for which the amplitude of the flux distribution is maximal. The main contributions will come from those trajectories whose action is minimized. This implies minimizing the sum of actions appearing in the exponent, with respect to two variables: the Wigner variable ξ and the location in phase space q. Variation of the actions with respect to the Wigner variable ξ gives the condition

$$p_f\left(q+\frac{\xi^*}{2},q_{DS}\right)=p_f\left(q-\frac{\xi^*}{2},q_{DS}\right), \tag{2.11}$$

where the notation p_f implies the final momentum and ξ^* is that value of the variable ξ for which Eq. (2.11) is obeyed. In

words, this result implies equality of the final momenta of the two trajectories that originate at the dividing surface and are propagated a time $\hbar\beta/2$.

Varying the action with respect to the location in phase space q gives a second condition

$$p_f\left(q^*+\frac{\xi^*}{2},q_{DS}\right)=-p_f\left(q^*-\frac{\xi^*}{2},q_{DS}\right), \quad (2.12)$$

implying that the final momenta have opposite signs. The two conditions, given in Eqs. (2.11) and (2.12), can be obeyed simultaneously if and only if the final momenta are zero. Thus the two contributing trajectories must end at turning points.

Finally, one may also vary the location of the dividing surface. This is the heart of variational rate theory. In classical mechanics, one knows that classical transition state theory (TST) will lead to an upper bound. In the quantum case, all that one can do is to demand that in any approximate theory the rate be extremal with respect to the location of the dividing surface since the exact rate is independent of the location [21,23]. This gives the third and final condition

$$p_i\left(q^*+\frac{\xi^*}{2},q_{DS}^*\right)=-p_i\left(q^*-\frac{\xi^*}{2},q_{DS}^*\right). \quad (2.13)$$

The initial momenta must have the same magnitude but opposite signs; therefore, they must have the same energy and so they lie on the same trajectory. This third condition identifies the location of the dividing surface as that point for which the time $(\hbar\beta/2)$ it takes to reach either of the turning points on the inverted potential is equal. In an asymmetric potential, the optimal dividing surface is temperature dependent and will always tend towards the ''soft'' part of the potential. To summarize, the three conditions imply that the main orbit that contributes to the flux distribution is periodic, with period $2\hbar\beta$, that the maximum in the configuration space will occur at the point q^*, which is halfway between the two turning points of the orbit, and that the optimal location of the dividing surface is at the point that is halfway in time between the two turning points.

C. The high-temperature ($\hbar\beta\omega^{\ddagger}\leqslant\pi$) semiclassical flux distribution

For a typical anharmonic potential, when inverted, the period is shortest at low energy and increases monotonically with the energy. The harmonic frequency of the inverted potential is $\omega^{\ddagger}$ [cf. Eq. (2.2).] For temperatures such that $\hbar\beta/2<\pi/2\omega^{\ddagger}$ there does not exist a trajectory that can fulfill all three conditions, except for the trivial one, which sits at the minimum of the inverted potential energy. The threshold for the appearance of a nontrivial periodic solution is for temperatures such that $\hbar\beta\omega^{\ddagger}>\pi$ [27,28]. In this subsection we will derive the semiclassical symmeterised flux distribution in the high-temperature region, defined as $\hbar\beta\omega^{\ddagger}\leqslant\pi$. The low-temperature distribution will be considered in Sec. II D.

To obtain the flux distribution, one expands around the optimized points q^*, ξ^*, and q_{DS}^* up to quadratic terms

$$\begin{aligned}S\left(q+\frac{\xi}{2},q_{DS}^*\right)+S\left(q-\frac{\xi}{2},q_{DS}^*\right)&\\ \sim S\left(q^*+\frac{\xi^*}{2},q_{DS}^*\right)+S\left(q^*-\frac{\xi^*}{2},q_{DS}^*\right)&\\ +\left(\frac{1}{4}(\xi-\xi^*)^2+(q-q^*)^2\right)\frac{\partial\overline{p_f}}{\partial q_f}+o(q^4,\xi^4),&\end{aligned} \quad (2.14)$$

where we used the shorthand notation

$$\frac{\partial\overline{p_f}}{\partial q_f}\equiv\frac{1}{2}\left(\frac{\partial p_f\left(q^*+\frac{\xi^*}{2},q_{DS}^*\right)}{\partial q^*}+\frac{\partial p_f\left(q^*-\frac{\xi^*}{2},q_{DS}^*\right)}{\partial q^*}\right). \quad (2.15)$$

The derivative $\partial\overline{p_f}/\partial q_f$ plays a crucial role. If it is negative, then the points q^*, ξ^*, and q_{DS}^* give a local *maximum* of the action and the expansion about it is meaningless. For high temperatures, such that $\hbar\beta\omega^{\ddagger}<\pi$, the derivative is positive when expanding about the origin, the dynamics is classical-like, and the small ξ expansion used in Ref. [21] is valid.

Exactly at the temperature $\hbar\beta\omega^{\ddagger}=\pi$ the derivative will go to zero [27,28]. At lower temperature, it will become positive when expanding around the imaginary time periodic orbit, but will be negative when expanding about the origin. At high temperatures, the flux distribution will be dominated by the parabolic barrier; at low temperatures, the anharmonicity comes into play and the flux is dominated by the imaginary time periodic orbit.

At high temperature, all momenta are to be expanded around zero so that

$$\begin{aligned}p_i\left(q-\frac{\xi}{2},q_{DS}\right)-p_i\left(q+\frac{\xi}{2},q_{DS}\right)&\\ \sim-\xi\left.\frac{\partial p_i(q,q_{DS})}{\partial q}\right|_{q=0}+o(\xi^3).&\end{aligned} \quad (2.16)$$

Using the quadratic expansion for the action and integrating over the Wigner variable ξ one gets the expression [Eq. (3.18) of Ref. [21], given here for the sake of completeness]

$$\begin{aligned}&F(p,q;\hbar\beta\omega^{\ddagger}<\pi,q_{DS}=0)\\ &\simeq\frac{1}{2\pi\hbar m(\pi\hbar)^{1/2}}\frac{\left.\frac{\partial p_i(q,0)}{\partial q}\right|_{q=0}^2}{\left(\left.\frac{\partial p_f(q,0)}{\partial q}\right|_{q=0}\right)^{3/2}}p\\ &\times\exp\left[-\frac{1}{\hbar}\left(q^2\left.\frac{\partial p_f(q,0)}{\partial q}\right|_{q=0}+\frac{p^2}{\left.\frac{\partial p_f(q,0)}{\partial q}\right|_{q=0}}\right)\right].\end{aligned} \quad (2.17)$$

The partial derivatives are identical to those of a parabolic well whose frequency is $\omega^{\ddagger}$ and one readily finds that

$$\left.\frac{\partial p_i(q,0)}{\partial q}\right|_{q=0}=\frac{m\omega^{\ddagger}}{\sin(\hbar\beta\omega^{\ddagger}/2)}, \tag{2.18}$$

$$\left.\frac{\partial p_f(q,0)}{\partial q}\right|_{q=0}=\frac{m\omega^{\ddagger}}{\tan(\hbar\beta\omega^{\ddagger}/2)}. \tag{2.19}$$

The semiclassical flux distribution for high temperatures ($\hbar\beta\omega^{\ddagger}<\pi$) is identical to the exact quantum flux distribution for a parabolic barrier, as already given in Eq. (3.6) of Ref. [21]. The distribution has a single peak (in the upper half plane), located close to the barrier top. Note that the flux distribution differs from the product of the momentum and the Wigner representation of the operator $e^{-\beta H}$.

D. The low-temperature ($\hbar\beta\omega^{\ddagger}\geqslant\pi$) semiclassical flux distribution

The more interesting case is for low temperatures. The minimum action occurs for two trajectory segments, leading from q^*_{DS} to $q^*+\xi^*/2$ and leading from q^*_{DS} to $q^*-\xi^*/2$. One must sum over the two possible solutions for the Wigner variable: $\pm|\xi^*|$. The initial momentum is not zero and so to leading order

$$p_i\left(q-\frac{\xi}{2},q_{DS}\right)-p_i\left(q+\frac{\xi}{2},q_{DS}\right)\sim 2p_i\left(q^*-\frac{\xi^*}{2},q^*_{DS}\right)+2(q-q^*)\,\frac{\partial\Delta p_i}{\partial q_f}-(\xi-\xi^*)\,\frac{\partial\overline{p_i}}{\partial q_f}, \tag{2.20}$$

where we used the shorthand notation

$$\frac{\partial\Delta p_i}{\partial q_f}=\frac{1}{2}\left(\frac{\partial p_i\left(q^*-\frac{\xi^*}{2}\right)}{\partial q^*}-\frac{\partial p_i\left(q^*+\frac{\xi^*}{2}\right)}{\partial q^*}\right), \tag{2.21}$$

$$\frac{\partial\overline{p_i}}{\partial q_f}=\frac{1}{2}\left(\frac{\partial p_i\left(q^*-\frac{\xi^*}{2}\right)}{\partial q^*}+\frac{\partial p_i\left(q^*+\frac{\xi^*}{2}\right)}{\partial q^*}\right). \tag{2.22}$$

The momentum difference in Eq. (2.20) must be expanded up to first order. Around the crossover region $\hbar\beta\omega^{\ddagger}\simeq\pi$ the initial momentum p_i is small and the first-order term in $\xi-\xi^*$ becomes significant. For a symmetric potential the middle term on the right-hand side of Eq. (2.20) is zero by symmetry. Since the first-order term is important mainly in the vicinity of the crossover temperature, the middle term will usually be small unless the potential is extremely asymmetric. Henceforth, it will be ignored. Second- and higher-order terms in the expansion remain small at any temperature.

Using the Gaussian truncation for the action as in Eq. (2.14), integrating over the Wigner variable ξ in Eq. (2.10), and summing the contributions of both pairs of trajectories leads to the central result of this subsection:

$$\begin{aligned}F(p,q;\hbar\beta\omega^{\ddagger}>\pi,q^*_{DS})&\simeq\frac{1}{m(\pi\hbar)^{3/2}}\frac{\left|\frac{\partial p_i}{\partial q_f^{+}}\right|^{1/2}\left|\frac{\partial p_i}{\partial q_f^{-}}\right|^{1/2}}{\left(\frac{\partial\overline{p_f}}{\partial q_f}\right)^{1/2}}\\&\times\exp\left[-\frac{1}{\hbar}\,S\left(q^*+\frac{|\xi^*|}{2},q^*-\frac{|\xi^*|}{2};\hbar\beta\right)\right]\\&\times\exp\left(-\frac{p^2}{\hbar\,\frac{\partial\overline{p_f}}{\partial q_f}}-\frac{\partial\overline{p_f}}{\partial q_f}\,\frac{(q-q^*)^2}{\hbar}\right)\\&\times\left[|p_i|\sin\left(\frac{p|\xi^*|}{\hbar}\right)+p\,\frac{\partial\overline{p_i}/\partial q_f}{\partial\overline{p_f}/\partial q_f}\cos\left(\frac{p\xi^*}{\hbar}\right)\right],\end{aligned} \tag{2.23}$$

where we have abbreviated the notation and the $\pm$ signs indicate the momentum at $q^*\pm\xi^*/2$, etc. Note the difference between this result and the high-temperature distribution. The dependence on the momentum is sinusoidal at low temperatures, leading to alternate regions of positive and negative flux. At high temperatures, the flux is positive for positive momentum and negative for negative momentum, as might have been expected from a classical-like limit. In the deep tunneling region, this classical behavior disappears.

For extremely low temperatures, the period of the optimal path goes to infinity as the trajectory approaches the asymptotic region of the potential infinitely slowly. In this limit, the partial derivative $\partial\overline{p_f}/\partial q_f\to 0$ and the saddle point expansion becomes invalid. This deterioration in the quality of the semiclassical expansion will be demonstrated explicitly for the symmetric Eckart barrier potential in Sec. IV.

As is evident from the discussion thus far, at the temperature $\hbar\beta\omega^{\ddagger}=\pi$ a bifurcation occurs. At high temperature, one has a single minimum of the action, located at the bottom of the well. At the bifurcation point, this minimum turns into a maximum, but two new minima appear, located on opposite sides of the well bottom. In the vicinity of this bifurcation the standard semiclassical estimate of the propagator as given in Eq. (2.6) is no longer valid. Grabert and co-workers [27,28] have discussed in detail the appropriate uniform approximation for the propagator that must be employed. Such a theory may be carried out, but the fourth-order expansion of the action that leads to the uniform expression prevents analytic integration and leads to more complicated expressions [27,28].

III. THE SEMICLASSICAL LIMIT OF THE PROJECTION OPERATOR

A. Preliminaries

The matrix element of the propagator in the semiclassical limit takes the form

$$\langle q''|e^{-i\hat{H}t/\hbar}|q'\rangle_{\rm sc}=\sum_{\rm cl\ paths}\left(\frac{1}{2\pi i\hbar}\right)^{1/2}\left(\frac{\partial^2 W(q'',q';t)}{\partial q''\partial q'}\right)^{1/2}\times\exp\left(\frac{i}{\hbar}\,W(q'',q';t)-\frac{i\nu\pi}{2}\right), \tag{3.1}$$

where the sum is over all classical trajectories that start at time $t=0$ at the point q' and end at time t at the point q'' and ν is the Maslov index. The Lagrangian action $W(q'',q';t)$ is

$$W(q'',q';t)=\int_0^t L(q'',q')dt$$
$$=\int_{q'}^{q''} dq\sqrt{2m[E(q'',q',t)-V(q)]}$$
$$-E(q'',q',t)t \tag{3.2}$$

and $E(q'',q',t)$ is the classical energy of the trajectory. The semiclassical limit of the Wigner representation of the projection operator, taken at some fixed time t, is

$$P(p,q;t)=\left(\frac{1}{2\pi\hbar}\right)^2\int_0^\infty dq'\int_{-\infty}^{\infty}d\xi\, e^{ip\xi/\hbar}$$
$$\times\left(\frac{\partial^2 W\left(q-\frac{\xi}{2},q',t\right)}{\partial\left(q-\frac{\xi}{2}\right)\partial q'}\frac{\partial^2 W\left(q',q+\frac{\xi}{2},t\right)}{\partial q'\partial\left(q+\frac{\xi}{2}\right)}\right)^{1/2}$$
$$\times\exp\left\{\frac{i}{\hbar}\left[W\left(q',q+\frac{\xi}{2},t\right)-W\left(q-\frac{\xi}{2},q',t\right)\right]\right\}, \tag{3.3}$$

where we have ignored the Maslov index as it will not be important in the one-dimensional theory presented in this paper.

To simplify the ensuing analysis, it is convenient to use the symmetry of the action with respect to the exchange of the end points and rewrite Eq. (3.3) as

$$P(p,q;t)=\left(\frac{1}{2\pi\hbar}\right)^2\int_0^\infty dq'\int_{-\infty}^{\infty}d\xi\, e^{ip\xi/\hbar}$$
$$\times\left(\frac{\partial^2 W\left(q',q-\frac{\xi}{2},t\right)}{\partial\left(q-\frac{\xi}{2}\right)\partial q'}\frac{\partial^2 W\left(q',q+\frac{\xi}{2},t\right)}{\partial q'\partial\left(q+\frac{\xi}{2}\right)}\right)^{1/2}$$
$$\times\exp\left\{\frac{i}{\hbar}\left[W\left(q',q+\frac{\xi}{2},t\right)-W\left(q',q-\frac{\xi}{2},t\right)\right]\right\}. \tag{3.4}$$

We note that Eqs. (2.8) and (2.9) hold also in real time. The initial momentum of the trajectory starting at $q\pm\xi/2$ will be denoted $p_i^{\pm}(q',q\pm\xi/2,t)$, or in short $p_i^{\pm}$, and the final momentum will be denoted $p_f^{\pm}$.

B. Stationary phase estimate of the projection operator

The integration in Eq. (3.4) is over two variables: the Wigner coordinate ξ and the physical coordinate q', which is restricted to the interval $[0,\infty)$. The integration over both variables is to be made via stationary phase, expanding the actions up to second order about the stationary phase point (q'^*,ξ^*). The first variation with respect to q' gives

$$p_f^+-p_f^-=0. \tag{3.5}$$

This means that the final momentum of the two trajectories must be the same, at the same final point q'. The two trajectories are therefore identical, that is, $\xi^*=0$.

The first variation with respect to the Wigner variable ξ gives the second condition

$$p-\tfrac{1}{2}(p_i^++p_i^-)=0. \tag{3.6}$$

However, we already know from the first variation [Eq. (3.5)] that the two trajectories are identical; therefore, the second variation tells us that the initial momentum of the trajectory must be p. This simplifies the analysis. It means that for any fixed point in phase space (p,q), the stationary phase trajectory is the one that is initialized at that point and is evolved up to the time t. The point it reaches at time t is therefore q'^*. The fact that q' must be positive tells us that only those trajectories that end up at time t with positive final coordinate will contribute to the semiclassical projection operator.

The second variations of the exponents appearing in Eq. (3.4) are

$$\frac{\partial^2(W^+-W^-)}{\partial q'^2}=\frac{\partial p_f^+}{\partial q'}-\frac{\partial p_f^-}{\partial q'}=0, \tag{3.7}$$

$$\frac{\partial^2(W^+-W^-)}{\partial q'\partial\xi}=\frac{1}{2}\left(\frac{\partial p_f^+}{\partial q_i^+}+\frac{\partial p_f^-}{\partial q_i^-}\right)=\frac{\partial p_f}{\partial q_i}, \tag{3.8}$$

$$\frac{\partial^2(W^+-W^-)}{\partial\xi^2}=-\frac{1}{4}\left(\frac{\partial p_i^+}{\partial q_i^+}-\frac{\partial p_i^-}{\partial q_i^-}\right)=0. \tag{3.9}$$

Since expansion of the action around $q'^*,\xi=0$ gives to second order only the term $(q'-q'^*)\xi$, one can immediately integrate over the ξ variable in Eq. (3.4) to obtain a Dirac δ function, whose argument is $(q'-q'^*)(\partial p_f/\partial q_i)$. Note also that on the stationary phase trajectory, the prefactor is

$$\left(\frac{\partial^2 W\left(q',q-\frac{\xi}{2},t\right)}{\partial\left(q-\frac{\xi}{2}\right)\partial q'}\frac{\partial^2 W\left(q',q+\frac{\xi}{2},t\right)}{\partial q'\partial\left(q+\frac{\xi}{2}\right)}\right)^{1/2}\Bigg|_{q'=q'^*,\xi=0}$$
$$=\frac{\partial p_f}{\partial q_i}. \tag{3.10}$$

Therefore integration over q' leads to the simple result

$$P(p,q;t)=\frac{1}{2\pi\hbar}\,h(q'^*,t). \tag{3.11}$$

In other words, the projection operator projects onto all those phase space points (p,q) that when evolved a time t lead to a positive final value of the coordinate.

It is at this point that we take the infinite time limit ($t\to\infty$). Clearly, in this limit, all trajectories on one side of the classical separatrix lead to products, while those on the other side lead to reactants. Therefore the infinite time limit of Eq. (3.11) is just the classical projection operator

$$P_{\rm cl}=\frac{1}{2\pi\hbar}\,h[p\pm\sqrt{-2mV(q)}], \tag{3.12}$$

where the plus sign is taken for positive q, the minus sign is taken for negative q, and the potential $V(q)$ is taken such that $q=0$ is the location of the barrier and $V(0)=0$.

It is possible in principle to go beyond the stationary phase result by expanding the action and the prefactor to higher orders in the variables $q'-q'^*,\xi$. This would lead to higher-order correction terms such as those derived in Ref. [23].

IV. SEMICLASSICAL RATE THEORY

A. Semiclassical rate theory for high temperatures

The semiclassical rate expression may be now obtained by replacing the exact projection operator, appearing in Eq. (1.8), with the classical projection operator, given in Eq. (3.12), and the exact quantum flux distribution by its semiclassical approximation, as given in Eqs. (2.17) and (2.23) for the high- and low-temperature limits, respectively. The integration over the momentum is analytical and one remains with a simple quadrature for the remaining integration over the coordinate. The resulting semiclassical rate expression for the high-temperature region is thus found to be

$$k(\hbar\beta\omega^{\ddagger}<\pi)_{\rm SCLMQCLT}$$
$$=Q_r(T)^{-1}\,\frac{1}{4m\pi\hbar}\,\sqrt{\frac{\hbar}{\pi}}\frac{\left(\dfrac{\partial p_i}{\partial q}\right)^2}{\sqrt{\dfrac{\partial p_f}{\partial q}}}\int_{-\infty}^{\infty}dq$$
$$\times\exp\left(-q^2\,\frac{\partial p_f}{\partial q}\Big/\,\hbar\right)\exp\left[2mV(q)\Big/\left(\hbar\,\frac{\partial p_f}{\partial q}\right)\right]. \tag{4.1}$$

The partial derivatives appearing in this expression have already been given in Eqs. (2.18) and (2.19).

For a parabolic barrier potential this result is exactly the parabolic barrier estimate for the rate

$$k_{\rm PB}=Q_r(T)^{-1}\,\frac{\omega^{\ddagger}}{4\pi\,\sin(\hbar\beta\omega^{\ddagger}/2)}. \tag{4.2}$$

In other words, if one uses the semiclassical quantum TST (SCLQTST) in which the exact projection operator is replaced by the parabolic barrier projection operator, the semiclassical rate theory reduces to the parabolic barrier approximation for the rate. Semiclassical transition state theory, in the high-temperature limit, is identical to the parabolic barrier estimate.

If, however, one uses the classical projection operator, the result is different. For example, for a symmetric potential, one will often find that the potential $V(q)$, which is the true potential, will be less negative than its parabolic barrier estimate. Therefore, the high-temperature semiclassical rate will be *larger* than obtained from the parabolic barrier result. Contrary perhaps to intuition, the parabolic barrier estimate for the rate is not an upper bound, even for the symmetric Eckart potential.

B. Semiclassical rate theory for low temperature

The low-temperature semiclassical rate expression is obtained by insertion of the low-temperature semiclassical flux [Eq. (2.23)] and the classical projection operator [Eq. (3.12)] into the exact rate expression [Eq. (1.8)]. The result is

$$k(\hbar\beta\omega^{\ddagger}>\pi)_{\rm SCLMQCLT}$$
$$=Q_r(T)^{-1}\,\frac{1}{(2m\pi\hbar)}\left|\frac{\partial p_i}{\partial q_f^{+}}\right|^{1/2}\left|\frac{\partial p_i}{\partial q_f^{-}}\right|^{1/2}$$
$$\times\exp\left[-\frac{1}{\hbar}\,S\left(q^*+\frac{|\xi^*|}{2},q^*-\frac{|\xi^*|}{2};\hbar\beta\right)\right](F_1+F_2), \tag{4.3}$$

where

$$F_1\equiv\left(|p_i|-\frac{|\xi^*|}{2}\,\frac{\partial\overline{p_i}}{\partial q_f}\right)e^{-(\xi^{*2}/4\hbar)S_2}$$
$$\times\frac{1}{2i}\int_{-\infty}^{\infty}dq\;e^{-[(q-q^*)^2/\hbar]S_2}$$
$$\times\left[\mathrm{erfc}\left(\frac{\sqrt{-2mV(q)}-i|\xi^*|\,\dfrac{S_2}{2}}{\sqrt{\hbar S_2}}\right)-\text{c.c.}\right], \tag{4.4}$$

$$F_2\equiv\sqrt{\frac{\hbar}{\pi S_2}}\,\frac{\partial\overline{p_i}}{\partial q_f}\int_{-\infty}^{\infty}dq\;e^{-(q-q^*)^2S_2/\hbar}e^{2mV(q)/\hbar S_2}$$
$$\times\cos\left(\frac{\xi^*}{\hbar}\,\sqrt{-2mV(q)}\right). \tag{4.5}$$

The erfc function is as defined in Ref. [29] and $S_2\equiv\partial\overline{p_f}/\partial q_f$.

One may insert here also the parabolic barrier potential $[V(q)=-\frac{1}{2}m\omega^{\ddagger 2}q^2]$ to regain the SCQTST expression. Note that at the bifurcation temperature $\hbar\beta\omega^{\ddagger}=\pi$ [27,28] the first contribution $F_1=0$, while the second contribution F_2 leads to an estimate that is exactly twice the estimate obtained from Eq. (4.1), which is based on the high-temperature limit. The low-temperature estimate includes contributions from two minima, the high-temperature only from one. If one restricts the integration over the Wigner variable ξ to the interval $[0,\infty)$ for the positive ξ^* trajectory and the interval $(-\infty,0]$ for the negative ξ^* trajectory, one obtains an approximate uniform expression that will give the correct factor at $\hbar\beta\omega^{\ddagger}=\pi$ and at lower temperature would reduce to the result given in Eqs. (4.3)–(4.5). As mentioned in Sec. II, the contribution F_2 is mainly important in the bifurcation region where $F_1\sim 0$. At much lower temperatures F_2 is substantially smaller than F_1.

The action appearing in the semiclassical TST rate expression is only half of the action of the full orbit, but the

period of the full orbit is $2\hbar\beta$. The rate estimate is still significantly lowered due to summation over the alternating signs of the flux. However, typically, at very low temperature, the semiclassical estimate (as well as the exact quantum TST and MQCLT estimates; see Refs. [21,23]) will remain somewhat larger than the exact rate. At high temperatures, the quantum TST rate estimate is similar to the classical and so again one has an upper estimate of the rate. It is therefore not very surprising that in practice, quantum TST and MQCLT lead to an estimate that is larger than the exact rate, irrespective of temperature.

C. Practical application: The symmetric Eckart potential

The Eckart barrier potential, defined such that the barrier energy is zero, has the form

$$V(q)=V^{\ddagger}\left(\frac{1}{\cosh^2(q/d)}-1\right). \tag{4.6}$$

The imaginary time dynamics occurs on the inverted potential whose Hamiltonian is

$$H=E=\frac{p^2}{2m}-\frac{V^{\ddagger}}{\cosh^2(q/d)}+V^{\ddagger}. \tag{4.7}$$

The well energy is zero and the frequency at the bottom of the well is $\omega^{\ddagger 2}=2V^{\ddagger}/md^2$. The time-dependent solution for a trajectory initiated at $t=0$ at the point (q_0,p_0) is

$$\sinh\left(\frac{q(t)}{d}\right)=\sinh\left(\frac{q_0}{d}\right)\cos(Ct)+\frac{p_0}{mdC}\cosh\left(\frac{q_0}{d}\right)\sin(Ct), \tag{4.8}$$

where the energy-dependent frequency C is

$$C(E)=\sqrt{\frac{2(V^{\ddagger}-E)}{md^2}}. \tag{4.9}$$

The solution given in Eq. (4.8) is valid for the energy range $0\leqslant E\leqslant V^{\ddagger}$.

The periodic orbit needed for the low-temperature flux distribution is initiated at $q_0=0$ and must end at time $t=\hbar\beta/2$ at the turning point, so that $p(\hbar\beta/2)=0$. The time dependence of this orbit simplifies to

$$\sinh\left(\frac{q(t)}{d}\right)=\frac{p_0}{mdC}\sin(Ct), \tag{4.10}$$

so that

$$p(t)=p_0\frac{\cos(Ct)}{\cosh\left(\frac{q(t)}{d}\right)}. \tag{4.11}$$

During the time $\hbar\beta/2$ the orbit performs a quarter of a full orbit; therefore, $C\hbar\beta/2=\pi/2$. This sets the temperature dependence of the energy of the orbit as $E=V^{\ddagger}-\pi^2md^2/2\hbar^2\beta^2$ or in dimensionless units

$$\frac{E}{V^{\ddagger}}=1-\frac{\pi^2}{\hbar^2\beta^2\omega^{\ddagger 2}}\equiv 1-\frac{1}{\nu^2}. \tag{4.12}$$

The dimensionless inverse temperature ν measures the energy; ν is allowed to vary between 1 (high temperature) and ∞ (zero temperature).

From Eqs. (4.10) and (4.11) one readily finds that

$$S_2\equiv\frac{\partial p_f}{\partial q_f}=\frac{\pi m\omega^{\ddagger}}{2}\frac{\nu^2-1}{\nu^3} \tag{4.13}$$

and

$$\frac{\partial p_i}{\partial q_f}=\frac{m\omega^{\ddagger}}{\nu^2}. \tag{4.14}$$

Evidently, when $\nu=1$, that is, when $\hbar\beta\omega^{\ddagger}=\pi$, the derivative S_2 vanishes. As expected, it also vanishes when $\nu\rightarrow\infty$, that is, in the limit of zero temperature.

For higher temperatures such that $\nu<1$, one is expanding about the trajectory that sits about the bottom of the well forever, that is, $q_0=p_0=0$. The second-order partial derivatives for this case are given in Eqs. (2.18) and (2.19).

In the low-temperature regime, the temperature-dependent location of the turning point is the solution of

$$\cosh\left(\frac{\xi^*}{2d}\right)=\nu. \tag{4.15}$$

The action of the trajectory initiated at $q=0$ ending at the turning point is

$$\begin{aligned}\frac{1}{\hbar}S\left(\frac{\xi^*}{2}\right)&=\frac{\pi d}{2\hbar}\left[\sqrt{2V^{\ddagger}}-\sqrt{2(V^{\ddagger}-E)}\right]-E\frac{\beta}{2}\\&=\frac{1}{2}\alpha\left(1-\frac{\nu}{2}-\frac{1}{2\nu}\right),\end{aligned} \tag{4.16}$$

where the dimensionless parameter $\alpha=\pi m\omega^{\ddagger}d^2/\hbar$. The classical dynamics may be expressed in terms of only the two reduced parameters ν and α.

Using the reduced coordinate $x=q/d$ and momentum $p_x=(d/\hbar)p$ one finds that up to a temperature-dependent normalization constant the semiclassical symmetrized thermal flux distribution in phase space [cf. Eq. (2.23)] becomes

$$\begin{aligned}&F(p_x,x;\hbar\beta\omega^{\ddagger}>\pi,q_{DS}=0)\\&\sim\left(\sin[2p_x\cosh^{-1}(\nu)]\right.\\&\quad\left.+\frac{p_x}{\alpha}\frac{2\nu^2}{(\nu^2-1)^{3/2}}\cos[2p_x\cosh^{-1}(\nu)]\right)\\&\quad\times\exp\left(-p_x^2\frac{2\nu^3}{\alpha(\nu^2-1)}-x^2\frac{\alpha(\nu^2-1)}{2\nu^3}\right).\end{aligned} \tag{4.17}$$

As mentioned in Sec. II, the prefactor of the cosine function becomes large as $\nu\rightarrow 1$ and becomes relatively small as $\nu\gg 1$. Plots of the resulting flux distributions are shown in Fig. 1 for the parameter values $\alpha=12$ and $\nu=2/\pi$, $5/\pi$, $7/\pi$, and $12/\pi$. The scale is the same as that of Fig. 1 of Ref. [23]. A comparison of the semiclassical flux distribution and the numerically exact quantum flux distributions as given in Ref.

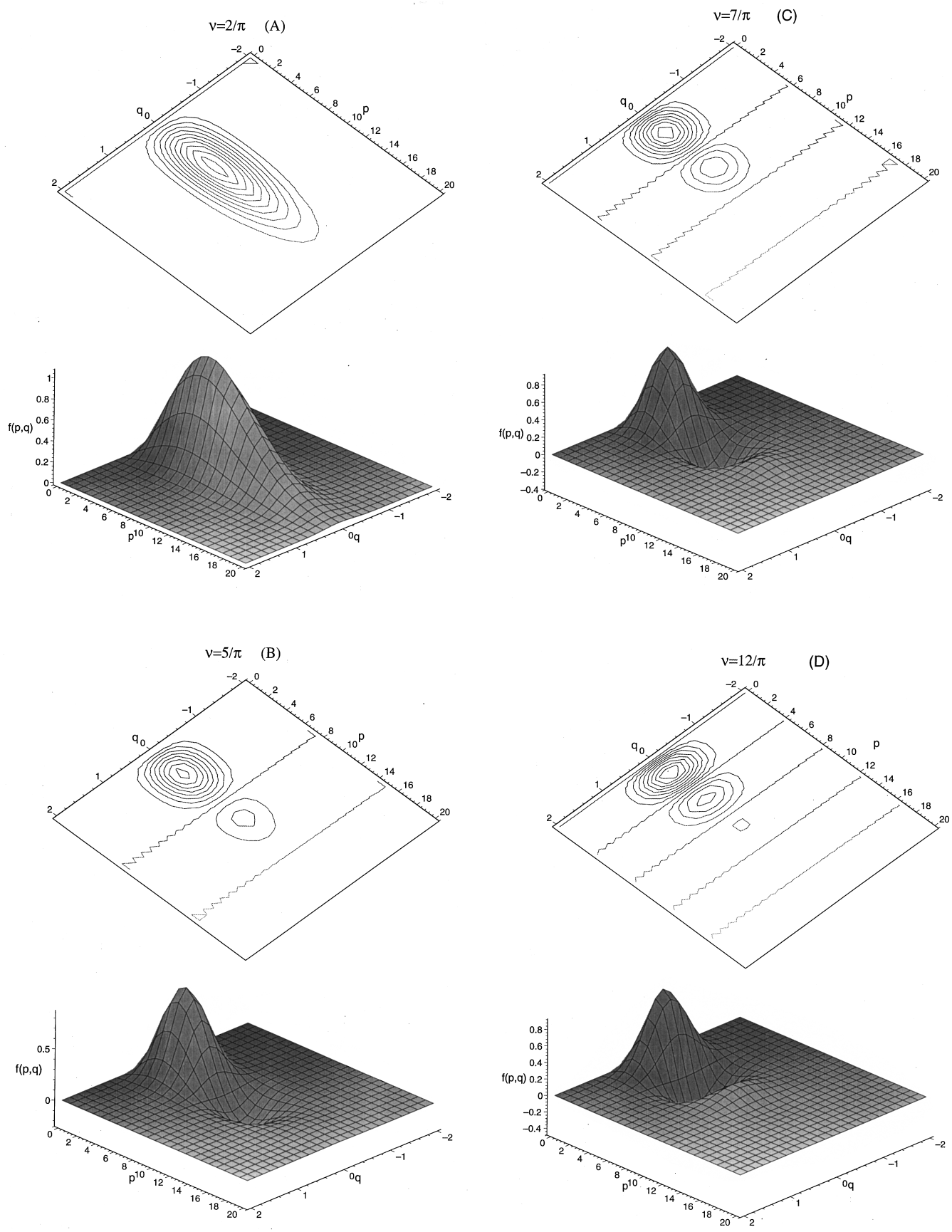

FIG. 1. Semiclassical flux distributions in phase space for the symmetric Eckart barrier potential ($\alpha=12$). Each of the four panels presents a 3D and a contour plot perspective of the distributions. The reduced temperature decreases going from $\hbar\beta\omega^{\ddagger}=2$ in (a) to $\hbar\beta\omega^{\ddagger}=12$ in (d). The coordinates are dimensionless and the scale is set to the one used in Fig. 1 of Ref. [23].

[23] shows that the semiclassical approximation manages to recover the quantum structure of the distributions.

The classical rate is $k_{\rm cl}=Q_r(T)^{-1}(1/2\pi\hbar\beta)$. Putting all this together, one finds that the semi-classical TST transmission coefficient for the symmetric Eckart barrier at low temperature is

$$P_{\rm SCLMQCLT}\equiv\frac{k_{\rm SCLMQCLT}}{k_{\rm cl}}(\hbar\beta\omega^{\ddagger}>\pi)=P_1+P_2, \tag{4.18}$$

$$\begin{aligned}P_1=&\frac{\alpha}{\nu}\left(\sqrt{1-\frac{1}{\nu^2}}-\frac{\cosh^{-1}(\nu)}{\nu^2}\right)\exp\left[\alpha\left(\frac{\nu}{2}-1+\frac{1}{2\nu}\right)\right]\\&\times\exp\left(-\cosh^{-2}(\nu)\,\frac{\alpha}{2}\,\frac{\nu^2-1}{\nu^3}\right)\\&\times i\int_0^{\infty}dx\,\exp\left(-x^2\,\frac{\alpha}{2}\,\frac{\nu^2-1}{\nu^3}\right)\\&\times\left[\mathrm{erfc}\left(\sqrt{1-\frac{1}{\cosh(x)^2}}\frac{\sqrt{2\alpha}}{\pi}\,\sqrt{\frac{\nu^3}{\nu^2-1}}\right.\right.\\&\left.\left.+i\,\cosh^{-1}(\nu)\sqrt{\frac{\alpha}{2}\,\frac{\nu^2-1}{\nu^3}}\right)-\mathrm{c.c.}\right],\end{aligned} \tag{4.19}$$

$$\begin{aligned}P_2=&2\sqrt{\frac{2\alpha}{\pi\nu^3(\nu^2-1)}}\exp\left[\alpha\left(\frac{\nu}{2}-1+\frac{1}{2\nu}\right)\right]\\&\times\int_0^{\infty}dx\,\exp\left(-x^2\,\frac{\alpha}{2}\,\frac{\nu^2-1}{\nu^3}\right)\exp\left[-\frac{2\alpha\nu^3}{\pi^2(\nu^2-1)}\right.\\&\left.\times\left(1-\frac{1}{\cosh(x)^2}\right)\right]\\&\times\cos\left(2\cosh^{-1}(\nu)\,\frac{\alpha}{\pi}\,\sqrt{1-\frac{1}{\cosh^2(x)}}\right).\end{aligned} \tag{4.20}$$

The transmission probability may be rewritten formally as

$$P=\int_0^{\infty}P(x)dx, \tag{4.21}$$

where $P(x)$ may be thought of as a coordinate-dependent transmission factor that if positive implies transmission to the product side and if negative to the reactant side. $P(x)$ is plotted vs x in Fig. 2(a) for $\nu=5/\pi$ and in Fig. 2(b) for $\nu=12/\pi$. Two curves are shown in each panel: The dashed line is obtained using the parabolic barrier separatrix and the solid line is obtained using the classical separatrix. One notes that the two curves are very similar. However, the most striking feature is that at the higher temperature [Fig. 2(a)] the main part of the curve is the positive component; the negative component of the curve is only half of the positive part.

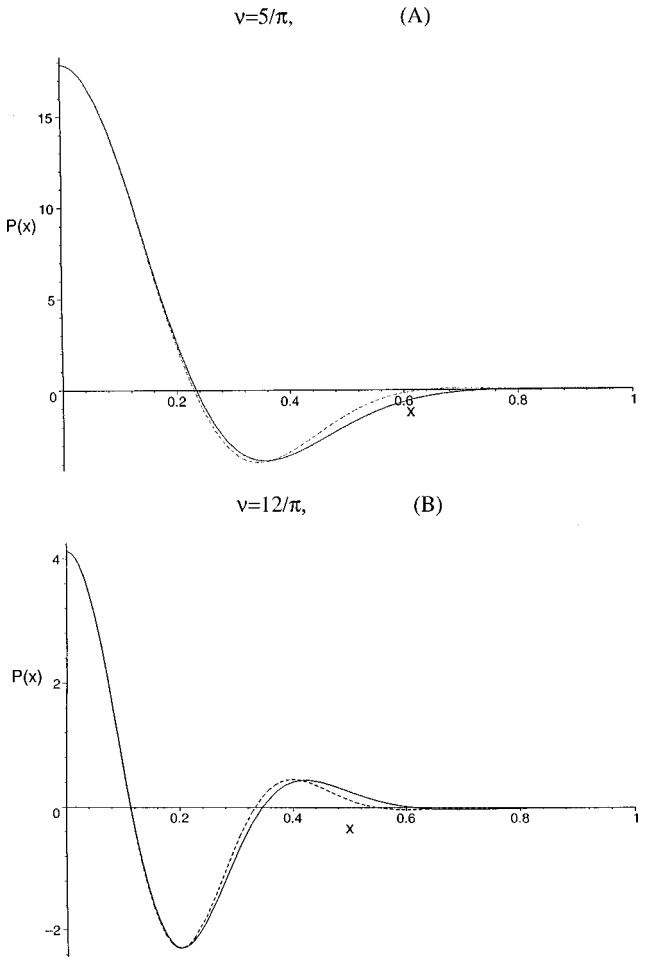

FIG. 2. Coordinate dependence of the semiclassical transmission probability. (a) corresponds to $\hbar\beta\omega^{\ddagger}=5$ and (b) to $\hbar\beta\omega^{\ddagger}=12$. $P(x)$ and x are in dimensionless units [in (b) $P(x)$ is in units of 10^5] such that the integral of the curves gives the transmission probability. In both panels the dashed line is obtained using the parabolic barrier projection operator and the semiclassical flux distribution and the solid line is obtained using the classical projection operator and the semiclassical flux distribution.

However, at low temperature, the negative part almost exactly cancels out the positive part and the net integral is only approximately 1% of the maximal value of the integrand at $x=0$.

A further comparison is given in Fig. 3 between the quantum transmission factor $P(x)$ computed from the product of the numerically exact quantum flux and the classical projection operator and its semiclassical approximation as obtained from Eqs. (4.18)–(4.20). One notes that the semiclassical theory is in good qualitative agreement at both temperatures shown. However, at $\nu=5/\pi$ the semiclassical theory is not quantitative in the close vicinity of the barrier. This is probably due to the fact that for this temperature range one should really employ the uniform theory of Weiper, Ankerhold, and Grabert [27,28] for the semiclassical density matrix because of the proximity to the bifurcation point $\hbar\beta\omega^{\ddagger}=\pi$.

The semiclassical transmission factor at high temperature is

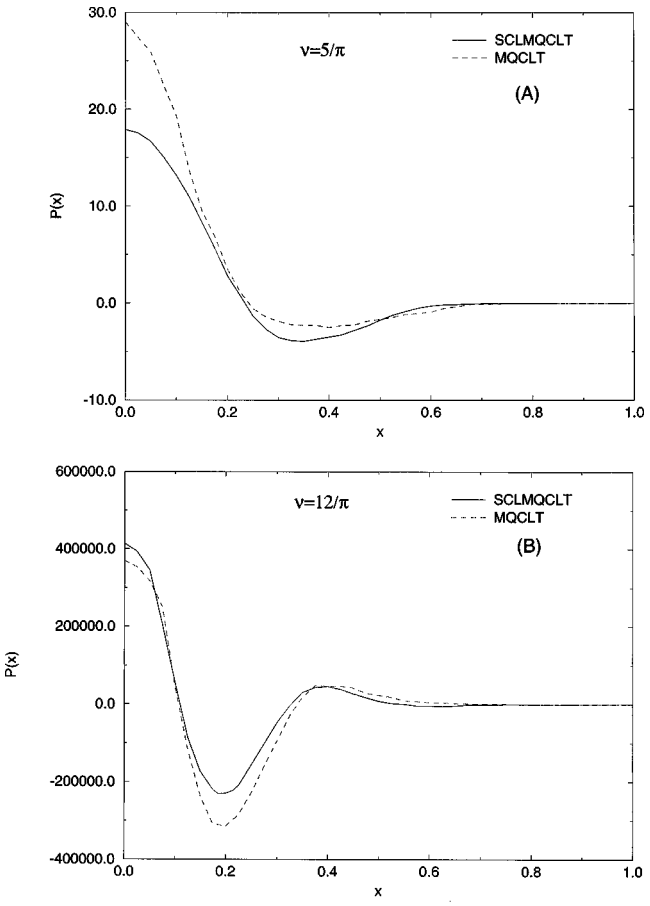

FIG. 3. Comparison of the semiclassical and quantum coordinate-dependent transmission probability. (a) corresponds to $\hbar\beta\omega^{\ddagger}=5$ and (b) to $\hbar\beta\omega^{\ddagger}=12$. In both panels the dashed line is obtained using the classical projection operator and the exact quantum flux distribution and the solid line is obtained using the classical projection operator and the semiclassical flux distribution.

$$\frac{k_{\mathrm{MQCLT}}}{k_{\mathrm{cl}}}(\hbar\beta\omega^{\ddagger}<\pi)=\frac{\nu\sqrt{\alpha\,\tan(\pi\nu/2)}}{\sin^2(\pi\nu/2)}\int_0^{\infty}dx\,\exp\times\left(-\frac{\alpha x^2}{\pi\,\tan(\pi\nu/2)}\right)\exp\left[-\frac{\alpha}{\pi}\tan(\pi\nu/2)\times\left(1-\frac{1}{\cosh^2(x)}\right)\right]. \tag{4.22}$$

A comparison between the semiclassical estimates and the quantum estimates for the transmission factor is provided in Table I and Fig. 4, using the value of $\alpha=12$. The semiclassical results for $\hbar\beta\omega^{\ddagger}\leqslant 3$ are based on Eq. (4.22) and the lower-temperature results are obtained using Eqs. (4.18)–(4.20). Above the bifurcation temperature of $\hbar\beta\omega^{\ddagger}=\pi$ the semiclassical results are in quantitative agreement with the quantum results. The semiclassical results obtained using the parabolic barrier approximation for the projection operator (SCLQTST) are identical to the parabolic barrier approximation. As discussed, they are *lower* than the results obtained using the classical projection operator (SCLMQCLT) and are lower than the exact rate.

For lower temperatures, the semiclassical theory is in qualitative agreement with the quantum computations. The quality of the semiclassical estimate deteriorates around the bifurcation temperature $\hbar\beta\omega^{\ddagger}=\pi$ and also for very low temperatures. The quality of the thermodynamic quantum theories based on numerically exact computation of the symmetrized thermal flux does not deteriorate as much in these limits, indicating that the error in the semiclassical approximation comes from inaccuracies in the evaluation of the symmetrized thermal flux distribution.

V. DISCUSSION

The semiclassical rate theory presented in this paper is an outgrowth of recent work on the formulation of a quantum

TABLE I. Comparison of semiclassical and quantum transmission coefficients for the symmetric Eckart barrier ($\alpha=12$).

$\hbar\beta\omega^{\ddagger}$	SCLQTST[a]	QTST[b]	SCLMQCLT[c]	MQCLT[d]	Exact[e]
1.5	1.10	1.13	1.13		1.13
2	1.19	1.23	1.24	1.27	1.22
3	1.50	1.54	1.52		1.52
4	1.49	2.09	1.49	2.16	2.07
6	2.45	5.74	2.20	5.75	5.20
8	14.0	29.3	11.9	26.2	21.8
10	176.0	248.0	149	235.0	162
12	3525	3058	3006	2700	1970
14	9.30×10^4		8.07×10^4		3.41×10^4
16	2.91×10^6		2.56×10^6		7.41×10^5
18	10.2×10^7		9.10×10^7		1.88×10^7
20	38.4×10^8	11.6×10^8	34.9×10^8	8.64×10^8	5.34×10^8

[a]SCLQTST is the semiclassical transmission coefficient using the parabolic barrier projection operator.

[b]QTST is the quantum transmission factor based on the numerically exact symmetrized thermal flux distribution and the parabolic barrier projection operator, adapted from Ref. [21].

[c]SCLMQCLT is the semiclassical transmission factor using the exact classical projection operator.

[d]MQCLT is the quantum transmission factor based on the numerically exact symmetrized thermal flux distribution and the exact classical projection operator, adapted from Ref. [23].

[e]Exact is the exact quantum mechanical transmission factor.

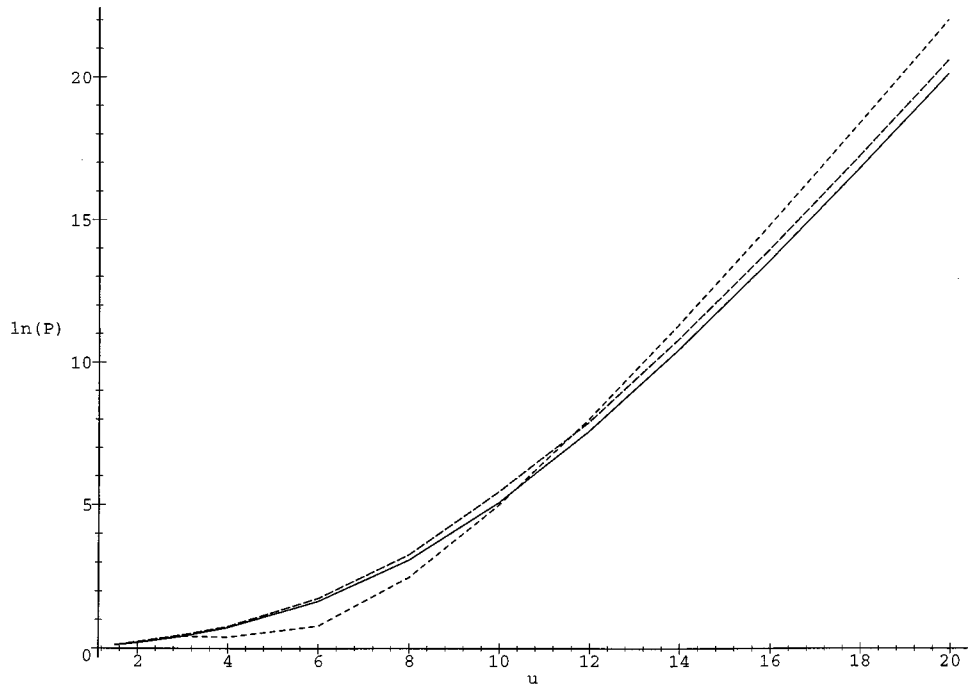

FIG. 4. Quantum and semiclassical thermal rate estimates for the symmetric Eckart barrier. The solid line is the exact quantum result, the dashed line is the MQCLT estimate, and the dotted line is the SCLMQCLT estimate (cf. Table I and the text). $u=\hbar\beta\omega^{\ddagger}$ and P is the transmission factor, defined as the ratio of the quantum and classical rates [cf., e.g., Eq. (4.18)].

thermodynamic theory of rates. In the quantum thermodynamic theory, the symmetrized thermal flux is computed numerically exactly and the projection operator is taken to be either the parabolic barrier projection operator (QTST) or the classical projection operator (MQCLT). Practical application of both approximations to the symmetric and asymmetric Eckart barrier leads to the following conclusions. (a) The low-temperature symmetrized thermal flux distribution is oscillatory in nature, with positive and negative contributions. (b) Both theories seem to bound the exact rate from above. (c) In the asymmetric case, the approximations are considerably improved by varying the location of the dividing surface of the flux operator, choosing the extremal location. (d) The differences between the two theories are not very big.

The semiclassical analysis presented in this paper goes a long way in explaining these findings. The oscillatory nature of the flux distribution is a direct consequence of the existence of the imaginary time periodic orbit contribution to the flux distribution. At temperatures above the bifurcation temperature $\hbar\beta\omega^{\ddagger}=\pi$, the flux distribution is localized about the barrier top and has a single positive peak in the upper half of the phase space plane. Lowering the temperature brings into play the imaginary time period orbit, whose action, length, and period increase with decreasing temperature. The increase in the length of the orbit is the main cause for the delocalization of the flux distribution and the formation of an oscillatory pattern.

Within the semiclassical theory, variation of the location of the dividing surface causes the smooth joining of the two trajectories that contribute to the flux, so that one remains with a single periodic orbit. Within the semiclassical theory, the difference between using the parabolic barrier separatrix or the classical separatrix is also not very big.

We have also presented a semiclassical analysis of the projection operator showing that a consistent use of the stationary phase approximation leads to the classical projection operator. This perhaps explains why use of the classical projection operator usually improves the thermodynamic quantum estimate for the rate, as shown in Ref. [23].

The semiclassical theory provides insight into the tunneling process. The small tunneling rate is the net remainder from a cancellation of the positive and negative parts of the flux distribution. At the same time, it is this cancellation that makes the semiclassical estimate difficult. Although the semiclassical theory does manage to account for the order of magnitude changes in the tunneling rate, it is not quantitative especially at low temperatures.

The analysis presented here is somewhat more complex than the theory based on finding the imaginary part of the free energy (Im F method) [1]. We note though that the Im F method is derived from first principles only for very low temperatures. It is exact at $T=0$ and at low temperatures the error obtained using this method is exponentially small [1,30,31]. However, as the temperature increases, the justification for the use of the instanton method disappears and one resorts to connection formulas derived by other methods [11] to provide a smooth transition from the low-temperature to the high-temperature regime. This deficiency does not exist in the present semiclassical theory, which is derived from first principles and is applicable for moderately low to high temperatures, the region where the instanton method is least well defined. The crossover from low to high temperatures is well understood and may be improved upon using a uniform theory for the action.

This paper dealt exclusively with one-dimensional tunneling. The methodology is generalizable to multidimensional systems. The three variations used in Sec. II to identify the periodic orbit will be generalized to a variation over all coordinates. This would lead again to a condition of zero momentum of the end points and a smooth joining of the trajectory on the dividing surface. The difference is that in the multidimensional case one may have in principle more than one trajectory that fulfills the conditions and one must sum over all the trajectories. A more detailed consideration of the thermodynamic rate theory in multidimensional systems will be given in Ref. [32].

ACKNOWLEDGMENTS

We thank Professor P. Hänggi and Dr. J.-L. Liao for stimulating discussions. This work has been supported by the Meitner-Humboldt Foundation (E.P.) and by grants from the Minerva Foundation, Munich, Germany, the U.S.–Israel Binational Science Foundation, and the German Israeli Foundation for Basic Research.

[1] P. Hänggi, P. Talkner, and M. Borkovec, Rev. Mod. Phys. **62**, 251 (1990), and references therein.
[2] *Dynamics of Molecules and Chemical Reactions*, edited by R. E. Wyatt and J. Z. H. Zhang (Dekker, New York, 1996).
[3] M. J. Gillan, J. Phys. C **20**, 3621 (1987).
[4] G. A. Voth, D. Chandler, and W. H. Miller, J. Chem. Phys. **91**, 7749 (1989).
[5] B. J. Berne and D. Thirumalai, Annu. Rev. Phys. Chem. **37**, 401 (1986).
[6] M. F. Herman and E. Kluk, Chem. Phys. **91**, 27 (1984).
[7] K. W. Kay, J. Chem. Phys. **101**, 2250 (1994).
[8] S. Keshavamurthy and W. H. Miller, Chem. Phys. Lett. **218**, 189 (1994).
[9] N. T. Maitra and E. J. Heller, Phys. Rev. Lett. **78**, 3035 (1997).
[10] N. T. Maitra and E. J. Heller, in *Classical, Semiclassical and Quantum Dynamics in Atoms*, edited by H. Friedrich and B. Eckhardt (Springer, Berlin, 1997), pp. 94–111.
[11] P. Hänggi and W. Hontscha, J. Chem. Phys. **88**, 4094 (1988).
[12] W. H. Miller, J. Chem. Phys. **62**, 1899 (1975).
[13] E. Wigner, Z. Phys. Chem. Abt. B **19**, 203 (1932).
[14] W. H. Miller, S. D. Schwartz, and J. W. Tromp, J. Chem. Phys. **79**, 4889 (1983).
[15] W. H. Thompson and W. H. Miller, J. Chem. Phys. **102**, 7409 (1995).
[16] T. J. Park and J. C. Light, J. Chem. Phys. **88**, 4897 (1988).
[17] T. Seideman and W. H. Miller, J. Chem. Phys. **95**, 1768 (1991).
[18] D. Brown and J. C. Light, J. Chem. Phys. **97**, 5465 (1992).
[19] D. H. Zhang and J. C. Light, J. Chem. Phys. **104**, 6184 (1995); **106**, 551 (1997).
[20] W. H. Thompson and W. H. Miller, J. Chem. Phys. **106**, 142 (1997).
[21] E. Pollak and J.-L. Liao, J. Chem. Phys. **108**, 2733 (1998).
[22] E. Wigner, Phys. Rev. **40**, 749 (1932).
[23] J. Shao, E. Pollak, and J.-L. Liao, J. Chem. Phys. **108**, 9711 (1998).
[24] H. Wang, X. Sun, and W. H. Miller, J. Chem. Phys. **108**, 9726 (1998).
[25] E. Pollak, J. Chem. Phys. **107**, 64 (1997).
[26] W. H. Miller, J. Chem. Phys. **58**, 1664 (1973).
[27] J. Ankerhold and H. Grabert, Physica A **188**, 568 (1992).
[28] F. J. Weiper, J. Ankerhold, and H. Grabert, J. Chem. Phys. **104**, 7526 (1996).
[29] M. Abramowitz and I. A. Stegun, *Handbook of Mathematical Functions* (Dover, New York, 1965).
[30] W. Hontscha, Ph.D. thesis, University of Augsburg, 1990 (unpublished).
[31] P. Hänggi and W. Hontscha, Ber. Bunsenges. Phys. Chem. **95**, 379 (1991).
[32] J.-L. Liao and E. Pollak, J. Chem. Phys. (to be published).